Boundary Currents at the Northern Edge of the Chukchi Sea at 166°W

Min Li[1,2,3] , Robert S. Pickart[2] , Peigen Lin[2,4] , Rebecca A. Woodgate[5] , Guiyuan Wang[1,3], and Lingling Xie[1,3]

[1]Laboratory of Coastal Ocean Variation and Disaster Prediction, College of Ocean and Meteorology, Guangdong Ocean University, Zhanjiang, China, [2]Woods Hole Oceanographic Institution, Woods Hole, MA, USA, [3]Key Laboratory of Space Ocean Remote Sensing and Application, Ministry of Natural Resources, Beijing, China, [4]School of Oceanography, Shanghai Jiao Tong University, Shanghai, China, [5]Applied Physics Laboratory, University of Washington, Seattle, WA, USA

Abstract Data from two moorings deployed at 166°W on the northern Chukchi shelf and slope from summer 2002 to fall 2004, as part of the Western Arctic Shelf-Basin Interactions program, are analyzed to investigate the characteristics and variability of the flow in this region. The depth-mean velocity at the outer-shelf mooring is northeastward and bottom-intensified, while that at the upper-slope mooring is northwestward and surface-intensified. This, together with results from a high resolution ocean and sea ice reanalysis, indicates that the outer-shelf mooring sampled the seaward edge of the Chukchi Shelfbreak Jet, while the upper-slope mooring sampled the shoreward edge of the Chukchi Slope Current. The coupled variability in velocity at both sites is related to the wind stress curl over the Chukchi Sea shelf, likely via Ekman dynamics and geostrophic set up, analogous to the dynamics of both currents closer to Barrow Canyon near 157°W. Hydrographic signals are analyzed to elucidate the origin of the water masses present at this location. It is argued that the annual appearance of Pacific-origin warm water at the outer-shelf (upper-slope) mooring in late-fall and winter originates from Herald (Barrow) Canyon some months earlier. Our results constitute the first robust evidence that the westward-flowing Chukchi Slope Current persists this far west of Barrow Canyon.

Plain Language Summary The boundary currents along the shelfbreak and slope of the Chukchi Sea play a key role in the regional ecosystem via advection and shelf-basin exchange of water and properties. Two-years of observational data obtained at two fixed locations on the Chukchi Shelfbreak and slope at 166°W revealed that the mean current in this region was northeastward on the outer shelf and northwestward at the upper slope. This is the signature of the Chukchi Shelfbreak Jet and Chukchi Slope Current, respectively, further verified using output from a high resolution ocean model over the same time period. The velocity at the two locations co-varies, driven predominantly by the changing rotation of the wind over the Chukchi shelf. Warm water was found annually in the fall/winter at the two locations. Using additional mooring data, it is argued that the warm water in the Chukchi Shelfbreak Jet stems from Herald Canyon in the west, while the warm water in the Chukchi Slope Current stems from Barrow Canyon in the east. Our results demonstrate for the first time that the Chukchi Slope Current persists far west of Barrow Canyon.

1. Introduction

The boundary current system along the northern Chukchi Shelfbreak and slope strongly influences the fate of Pacific-origin water in the western Arctic, and, as such, plays a vital role in the regional ecosystem. Its heat transport contributes to ice-melt in the basin (Shimada et al., 2006; Woodgate et al., 2010), its freshwater transport contributes to Arctic stratification and the Beaufort Gyre freshwater reservoir (Pickart et al., 2013; Steele et al., 2004), its nutrient transport supports the regional ecosystem (Hill & Cota, 2005; Jones & Anderson, 1986), and its transport of winter water ventilates the cold halocline of the Canada Basin (Spall et al., 2018). In order to quantify the shelf-basin exchange in this part of the Arctic, it is necessary to understand the structure, variability, and dynamics of this boundary current system.

To first order, the circulation of Pacific water in the Chukchi Sea is topographically steered. After passing through Bering Strait, the Pacific water generally follows three main branches (Figure 1): the western branch flowing through Hope Valley, the middle branch passing through the Central Channel, and the eastern branch flowing along the Alaskan coast (Weingartner et al., 2005). In summer to late fall, the eastern branch is dominated by
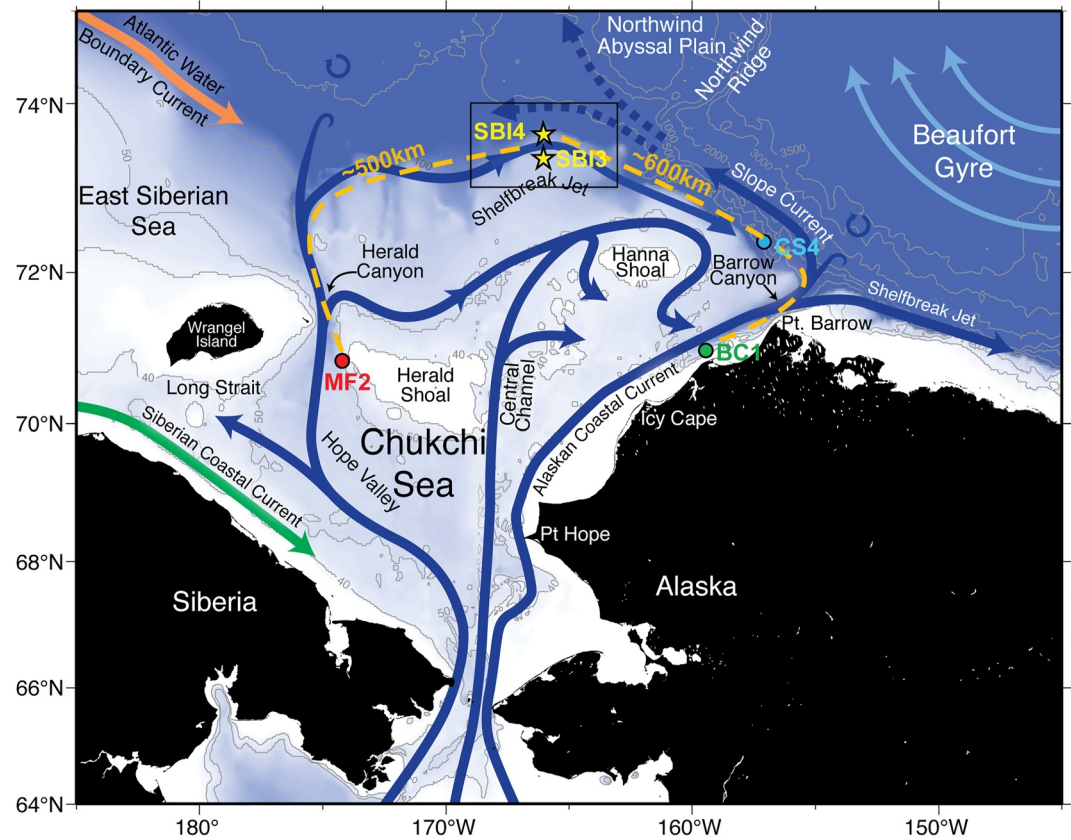
Figure 1. Schematic circulation of the Chukchi Sea (after Corlett & Pickart, 2017). The bathymetry is shaded (from ETOPO2), and place names are indicated. Locations of the moorings used in the study are shown: SBI3 and SBI4 (yellow stars), CS4 (cyan circle), BC1 (green circle), and MF2 (red circle). The black rectangle denotes the zoomed-in region in Figure 2a. The orange dashed lines show the approximate distances from MF2 to SBI3 and from BC1 to SBI4, which are used in Section 4.

the warm fresh waters of the Alaskan Coastal Current (Paquette & Bourke, 1974). Some of the water in the western branch flows through Herald Canyon (Pickart et al., 2010) and subsequently feeds the eastward-flowing Chukchi Shelfbreak Jet (Corlett & Pickart, 2017; Li et al., 2019; Linders et al., 2017; Mathis et al., 2007). Part of the western branch is also known to flow into the East Siberian Sea via Long Strait (Woodgate, Aagaard, & Weingartner, 2005). Most of the water in the central and eastern branches drains through Barrow Canyon (Gong & Pickart, 2015; Itoh et al., 2013; Weingartner et al., 2017), feeding both the eastward-flowing Beaufort Shelfbreak Jet along the northern shelf of Alaska and the westward-flowing Chukchi Slope Current (Corlett & Pickart, 2017; Li et al., 2019; Lin et al., 2021; Nikolopoulos et al., 2009; Pickart, 2004).

The Beaufort Shelfbreak Jet has been extensively investigated over the years through both observational and modeling studies. In the mean it is 10–15 km wide and bottom-intensified (e.g., Pickart, 2004). Seasonally it transports warm Pacific water eastward in summer and early-fall, and cold Pacific water during the remainder of the year. Using mooring data from 2002 to 2004, its volume transport was estimated to be 0.13 Sv (Nikolopoulos et al., 2009), but over the following decade the transport decreased by more than 80% (Brugler et al., 2014). The current is subject to baroclinic instability (Spall et al., 2008) and is strongly wind forced, leading to upwelling (e.g., Lin et al., 2019; Schulze & Pickart, 2012) and downwelling (e.g., Foukal et al., 2019).

The basic structure of the boundary current system west of Barrow Canyon has only recently been characterized through a combination of shipboard observations, Lagrangian measurements, mooring timeseries, and model studies. The two main components of flow are the eastward-flowing Chukchi Shelfbreak Jet and the westward-flowing Chukchi Slope Current. The Chukchi Shelfbreak Jet is bottom-intensified, centered near the 90 m isobath, with a similar structure to the Beaufort Shelfbreak Jet (Llinás et al., 2009; Mathis et al., 2007). It transports 0.01–0.1 Sv of Pacific water, with frequent current reversals due to variations in the wind stress

curl over the Chukchi shelf (Li et al., 2019). The current is known to spawn eddies of Pacific Water (Pickart et al., 2005), likely due to baroclinic instability (Spall et al., 2008). It is also subject to upwelling (Li et al., 2019; Mathis et al., 2007; Spall et al., 2014).

Seaward of the Chukchi Shelfbreak resides the Chukchi Slope Current, centered near the 250 m isobath. It is approximately 50 km wide and transports approximately 0.5 Sv of Pacific water, accounting for nearly half of the Pacific water that enters the Arctic through Bering Strait. The current primarily stems from the outflow of Barrow Canyon (Corlett & Pickart, 2017; Leng et al., 2021; Li et al., 2019). It is surface intensified in summer and fall, and mid-depth intensified in winter and spring when it is located ~10 km farther onshore (Leng et al., 2021; Li et al., 2019). Leng et al. (2022) argue that the mid-depth intensified structure is due to the different ice-ocean stress curl on the southern and northern sides of the Chukchi Slope Current, which drives an overturning circulation that displaces the isopycnals vertically, setting up a subsurface velocity maximum. Numerical modeling suggests that the seaward portion of the Chukchi Slope Current (roughly a third of the transport) is fed by water stemming from the Beaufort slope (Leng et al., 2021), with a connection to the Beaufort Gyre (Spall et al., 2018).

The mesoscale variability of the Chukchi Slope Current was investigated by Li et al. (2019) using mooring data from 157°W, roughly 100 km to the west of Barrow Canyon. They found that the slope current varied in concert with the nearby Chukchi Shelfbreak Jet. This was characterized by two extreme states: when the Chukchi Slope Current was especially strong, the Chukchi Shelfbreak Jet weakened or reversed to the west, and, conversely, when the Chukchi Shelfbreak Jet was particularly strong, the Chukchi Slope Current weakened, with reversed flow at depth. Li et al. (2019) used a regional numerical model together with a simple analytical theory to demonstrate that the two extreme states are driven by variations in the strong positive/negative wind stress curl on the shelf, which drives low/high sea level by divergence/convergence of the Ekman transport. This in turn affects the geostrophic current along the shelfbreak and slope. Farther offshore, however, near the 1,000 m isobath, data from a mooring revealed that the fluctuations of the flow deeper than ~40 m depth are not significantly correlated with the wind stress curl on the shelf or the wind along the slope. Instead they seem to be dynamically related to the extension of the southern edge of the Beaufort Gyre (Stabeno & McCabe, 2020).

To date, the downstream fate of the Chukchi Slope Current is not fully determined. Evidence from both observations and models suggest that the current bifurcates as it progresses westward from Barrow Canyon. Shipboard velocity measurements and trajectories of satellite-tracked drifters reveal that part of the current persists westward along the slope to the vicinity of 165°–168°W (Corlett & Pickart, 2017; Stabeno et al., 2018; Stabeno & McCabe, 2020). At the same time, additional drifter data and float measurements indicate that a portion of the current is diverted to the north around 162°W into the Chukchi Borderland (Boury et al., 2020; Stabeno et al., 2018). In particular, all five profiling floats released in the Chukchi Slope Current near 160°W and tracked by Boury et al. (2020) left the continental slope in the vicinity of the Northwind Abyssal Plain. Such a bifurcation of the Chukchi Slope Current is supported by the numerical modeling results of Leng et al. (2021), who showed that the portion of the slope current along the deeper isobaths veers northward beyond the Northwind Ridge and gets entrained into the Beaufort Gyre, while the portion of the current on the upper slope continues flowing to the west toward the East Siberian Sea. This is consistent with the lateral distribution of Pacific Summer Water presented in Lin et al. (2021) using historical hydrographic data. Lin et al. (2021) further argued that these pathways are dynamically influenced by the extent and strength of the Beaufort Gyre, with more Pacific summer water carried westward by the Chukchi Slope Current when the Beaufort Gyre is expanded (Lin et al., 2021).

At this point it is unclear how far west the Chukchi Slope Current extends beyond Barrow Canyon, if the bifurcation of the current is time dependent, and if both of the bifurcated pathways are always present. It is also remains to be determined what drives the dominant variability of the flow at these longitudes and if the variability is similar to that near Barrow Canyon. Part of the difficulty is that most of the measurements of the current to date are based on synoptic shipboard observations or drifters, and long-term observations are lacking. In this paper, we present results from a 2-year deployment of two moorings on the continental slope of the Chukchi Sea from 2002 to 2004, west of the Canada Basin at 166°W. The hydrographic and velocity data are used to investigate the nature of the boundary current system at a location 300 km downstream of the 2013–2014 mooring array, which was previously used by Li et al. (2019) to describe the Chukchi Slope Current shortly after it emerges from Barrow Canyon. The paper is structured as follows. In Section 2, the data and methods used are introduced. Section 3 contains an analysis of the boundary current system, including its mean structure and temporal
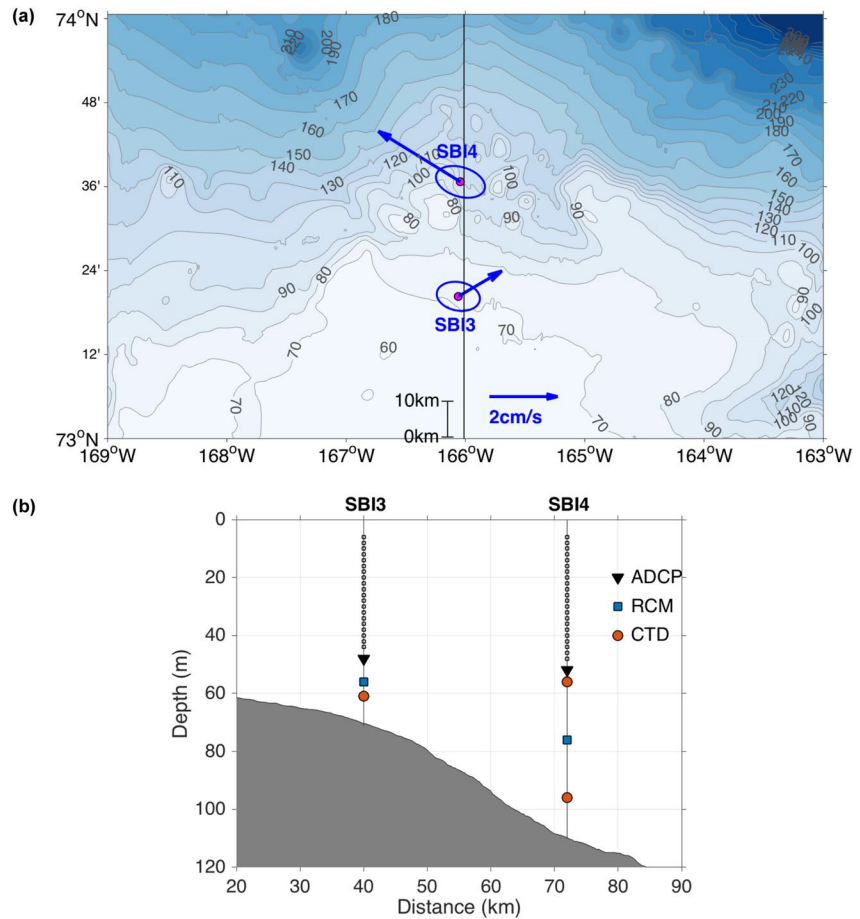
Figure 2. (a) Enlarged view of the study domain, corresponding to the black rectangle in Figure 1, including the 2-year depth-averaged mean velocity vectors and standard error ellipses (blue) at the two SBI moorings. The black line denotes the section along which shipboard bathymetric data were collected, with the origin at the southernmost location (73°N, 166°W) and the distance scale shown in the lower middle. The bathymetry (from IBCAOv3) is shaded. (b) Configuration of the two SBI moorings. The black triangle, blue square, and red circle denote the ADCP, RCM and CTD, respectively. The small black squares denote the depths of the ADCP bins. The bottom depth is from the shipboard echosounder observations along the 166°W section during the cruise in July 2002.

variability. Section 4 describes some hydrographic implications regarding the flow. The results are summarized in Section 5.

2. Data and Methods

2.1. Mooring Data

From July 2002 to September 2004, two moorings (SBI3 and SBI4) were deployed on the northern Chukchi Shelfbreak and slope at 166°W (Figure 2), with a recovery and redeployment in September 2003. The moorings were part of the western Arctic Shelf-Basin Interactions (SBI) program. The instrumentation consisted of upward-facing acoustic Doppler current profilers (ADCPs), SBE-16 conductivity-temperature-depth (CTD) recorders, and Aanderaa rotor current meters (RCMs, version RCM-7), with the configurations shown in Figure 2b. The ADCPs and RCMs were equipped with temperature sensors, and the RCMs included pressure sensors as well, except for the instrument on SBI3 during the first year. The ADCPs provided hourly profiles of velocity with a vertical resolution of 2 m. Both the RCMs and the CTDs sampled hourly. A detailed summary of the mooring information is contained in Table 1.

The ADCP data near the surface were removed because of the contamination resulting from the strong surface acoustic reflection, which is a well-documented issue (Teledyne, 2011). In our case, for a water depth of

Table 1
Mooring Information

Mooring ID	Latitude and longitude	Water depth (m)	Instrument	Duration	Instrument depth (m)	Sample interval (h)	Range depth (m)	Bin depth (m)	Related studies
SBI3 (2002–2003)	73°20.3′N 166°3.6′W	71	ADCP	7/21/2002–9/16/2003	48	1	6–44	2	–
			RCM	7/21/2002–9/16/2003	56	1	–	–	
			CTD	7/21/2002–9/16/2003	61	1	–	–	
SBI4 (2002–2003)	73°36.7′N 166°2.5′W	108	ADCP	7/22/2002–9/17/2003	52	1	6–48	2	–
			CTD	7/22/2002–9/17/2003	56	1	–	–	
			RCM	7/22/2002–9/17/2003	76	1	–	–	
			CTD	7/22/2002–9/17/2003	96	1	–	–	
SBI3 (2003–2004)	73°20.3′N 166°3.5′W	72	ADCP	9/18/2003–9/17/2004	48	1	6–44	2	–
			RCM	9/18/2003–9/17/2004	55	1	–	–	
			CTD	9/18/2003–9/17/2004	60	1	–	–	
SBI4 (2003–2004)	73°36.7′N 166°2.5′W	107	ADCP	9/17/2003–9/17/2004	52	1	6–48	2	–
			CTD	9/17/2003–9/17/2004	56	1	–	–	
			RCM	9/17/2003–9/17/2004	76	1	–	–	
			CTD	9/17/2003–9/17/2004	96	1	–	–	
BC1	71°3.1′N 159°32.8′W	78	RCM	8/4/2002–5/23/2003	64	1	–	–	Pisareva et al. (2019)
			CTD	8/3/2002–9/12/2003	67	1	–	–	
	71°3.1′N 159°32.5′W	79	RCM	9/15/2003–9/13/2004	64	1	–	–	
			CTD	9/15/2003–9/14/2004	67	1	–	–	
MF2	70°57.8′N 174°11.2′W	49	RCM	9/21/1990–9/30/1991	40	1	–	–	Woodgate, Aagaard, and Weingartner (2005)
			CTD	9/21/1990–10/2/1991	41.6	1	–	–	
CS4	72°23.1′N 157°8.8′W	249	CMP[a]	10/15/2013–09/21/2014	–	6	50–235	2	Li et al. (2019)
			ADCP	10/13/2013–09/22/2014	241	1	22–222	10	

[a]CMP is a coastal moored profiler which provides vertical profiles of temperature and salinity.

approximately 50 m, this meant removing the top three bins. The velocity data from the ADCP and RCM were 36-hr low-passed to remove tidal and inertial signals, and then rotated into alongstream and cross-stream directions, where the coordinate system was defined by the directions of the standard error ellipses at the two moorings (which is approximately along the isobaths). Positive alongstream u is toward the southeast (100.7°T, 107.2°T) and positive cross-stream v is toward the northeast (10.7°T, 17.2°T) at SBI3, SBI4, respectively. Standard error ellipses were computed using an integral time scale determined from the depth-averaged alongstream velocity at two moorings. The integral time scale is 5.2 and 5.0 days for SBI3 and SBI4, which corresponds to 75 and 79 degrees of freedom, respectively.

We also use data from three other moorings (see Figure 1): one at the head of Barrow Canyon (BC1) from 2002 to 2004 (Pisareva et al., 2019), one on the eastern flank of Herald Canyon (MF2) from 1990 to 1991 (Woodgate, Aagaard, & Weingartner, 2005), and one from the mooring array analyzed by Li et al. (2019) located on the Chukchi continental slope to the west of Barrow Canyon (CS4). These data are used to investigate the advection of water mass signals by the currents. Information regarding these ancillary moorings is shown in Table 1. The reader is referred to Pisareva et al. (2019), Woodgate, Aagaard, and Weingartner (2005), and Li et al. (2019) for more details of BC1, MF2, and CS4, respectively. The velocity data from these three moorings were low-passed with the same 36-hr filter as the velocity data from the SBI moorings.

2.2. Reanalysis Fields

The sea level pressure and 10-m wind field from the European Centre for Medium-Range Weather Forecasts (ECMWF) ERA5 reanalysis data set were used to investigate the atmospheric forcing (https://doi.org/10.24381/cds.adbb2d47). The spatial resolution is 0.25° in latitude and longitude, with a temporal resolution of 1 hr (subsampled to 3 hr for this study). The ERA5 monthly reanalysis data set from 1979 to 2020 were used for the climatology (https://doi.org/10.24381/cds.f17050d7).

To provide a broader context of the velocity structure in the vicinity of the moorings, the daily GLORYS12V1 ocean and sea-ice reanalysis product from Copernicus Marine Service (CMEMS) is used (https://doi.org/10.48670/moi-00021). This product is based on the Nucleus for European Modeling of the Ocean (NEMO) platform which assimilates altimetry data and in-situ temperature and salinity observations (Jean-Michel et al., 2021). The lateral resolution is 1/12° (hence eddy resolving) with 50 vertical levels. For the domain considered here, the vertical levels vary from ∼1 m at surface to ∼17 m at a depth of 100 m.

2.3. Ice Concentration Data

The ice concentration used is the OISST version2 Advanced Very High Resolution Radiometer (AVHRR) product from the National Oceanic and Atmosphere Administration/National Climatic Data Center (NOAA/NCDC; https://iridl.ldeo.columbia.edu/SOURCES/.NOAA/.NCDC/.OISST/.version2/.AVHRR/.ice/). The daily data have a spatial resolution of 0.25°.

2.4. EOF Analysis

A coupled empirical orthogonal function (EOF) analysis is done on the anomaly of the alongstream velocity profiles at SBI3 and SBI4 to determine the dominant variability in Section 3.4. The EOF method identifies statistical modes and principal components (PCs) of behavior of the variables and is widely applied in analyzing spatial and temporal variability of data (Emery & Thomson, 2001). The EOF modes describe spatial patterns and the PCs describe the associated temporal variability. For the mooring data used in the paper, the dominant mode (EOF1, PC1) explained roughly 70% of the variance, and the second mode was therefore not considered (see Section 3.4). To more clearly show what the EOF modes depict physically, two representative configurations of the alongstream velocity field are reconstructed by multiplying the structure of the EOF mode and positive/negative one standard deviation of its PC. This gives the dominant anomaly, which is then added to the 2-year mean profile. The reconstructed fields represent the two opposite states of the given mode (state I and II). This reconstruction method has been used in many previous studies (e.g., Håvik et al., 2017; Pickart, 2004).

3. Boundary Current System

3.1. Wind Forcing and Ice Cover

To set the environmental context, we begin with a short description of the wind forcing and sea-ice concentration during the mooring deployment period. Climatologically, the dominant winds are easterly/northeasterly (Figure 3a). During the 2-year study period the winds were predominantly out of the east, with frequent occurrences (15.2% of the duration) of northeasterly and southeasterly wind stronger than 8 m s^{-1} (Figure 3b), which is typical for the region when compared to the climatology (Figure 3a). Although less frequent, there were also strong westerly wind events with speeds up to 12 m s^{-1}, which are slightly more anomalous in light of the climatology. During each of the years, the ice concentration remained greater than 80% for more than 7 months. Freeze-up began in October for both years (with a short interruption in 2003), while melt-back began in mid-June for both years (Figure 3c). The ice melt season during the 2 years is typical of conditions since the 2000s, being longer than that in the 1980s and 1990s, consistent with the well-known long-term negative trend of sea ice in the Arctic (e.g., IPCC Special Report on Ocean and Cryosphere, 2019; Onarheim et al., 2018).

3.2. Mean Fields

The 2-year depth-averaged mean flow was oppositely directed at the two SBI mooring sites (Figure 2a): at the outer-shelf site (SBI3) the mean flow was less than 2 cm s^{-1} to the northeast (59.7°T), while at the upper-slope site
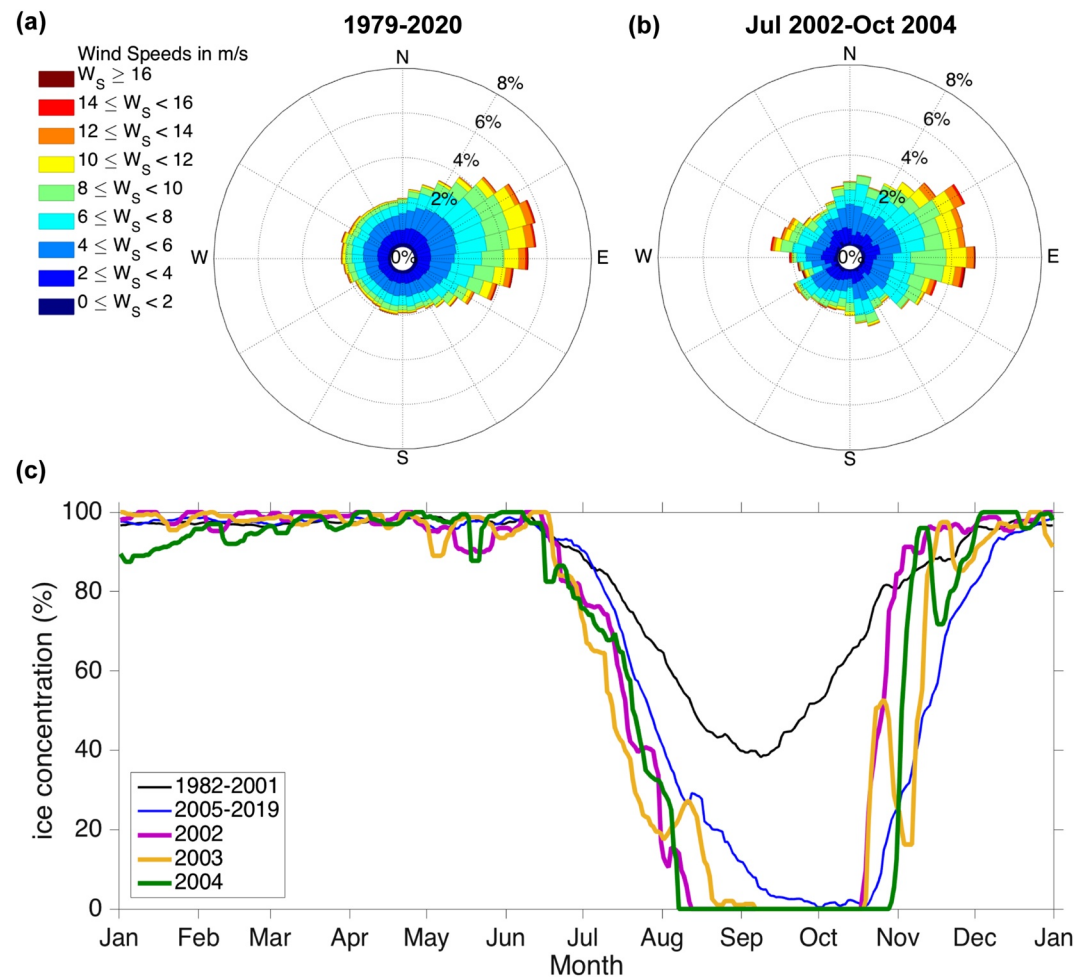
Figure 3. Climatological wind rose (a) from 1979 to 2020, and (b) during the study period. The direction of the wind rose is where the wind blows from, following meterological convention. (c) Daily ice concentration at the mooring site for the SBI years (2002: purple; 2003: orange; 2004: green), and the climatological mean during the years prior to (black) and subsequent to (blue) the mooring deployments.

(SBI4) it was approximately 3 cm s^{-1} to the northwest (121.6°T). The direction of the major axis of the standard error ellipse (100.7°T at SBI3 and 107.2°T at SBI4) was close to that of the mean vector at SBI4, while the two directions were considerably different at SBI3. The reason for this is that the depth-averaged flow at SBI3 varied predominantly between southeastward and northwestward (the direction of the major axis of the standard error ellipse).

The 2-year mean vertical profiles of alongstream velocity reveal a bottom-intensified southeastward current at SBI3 and a surface-intensified northwestward current at SBI4 (Figure 4a). The alongstream velocity at SBI3 was northwestward above 12 m with a velocity maximum of -0.9 ± 0.4 cm s^{-1} at the top ADCP bin (6 m). (The error bars presented in the paper are standard errors.) Below 12 m the alongstream flow reversed with a maximum of 2.0 ± 0.6 cm s^{-1} at the deepest ADCP measurement level of 44 m (27 m above the bottom). The RCM data showed a similar speed (2.0 ± 0.6 cm s^{-1}) at ~55 m, suggesting little shear in the deep part of the water column. At SBI4, the alongstream velocity was surface intensified, flowing to the northwest throughout the measurement range of the ADCP (above 48 m), with a maximum velocity of -4.8 ± 0.7 cm s^{-1} at the top bin (6 m). The flow weakens to -1.0 ± 0.8 cm s^{-1} at the deepest ADCP bin. The RCM data revealed a very weak mean southeastward current (0.2 ± 0.7 cm s^{-1}) with relatively large fluctuations at 76 m.

The vertical structure of the mean flow at the two mooring sites from the GLORYS reanalysis product, for the same 2-year period, is remarkably consistent with the mooring data (Figure 4a). To provide a broader spatial context, the mean vertical section of alongstream velocity at 166°W for July 2002 to September 2004 from GLORYS is shown
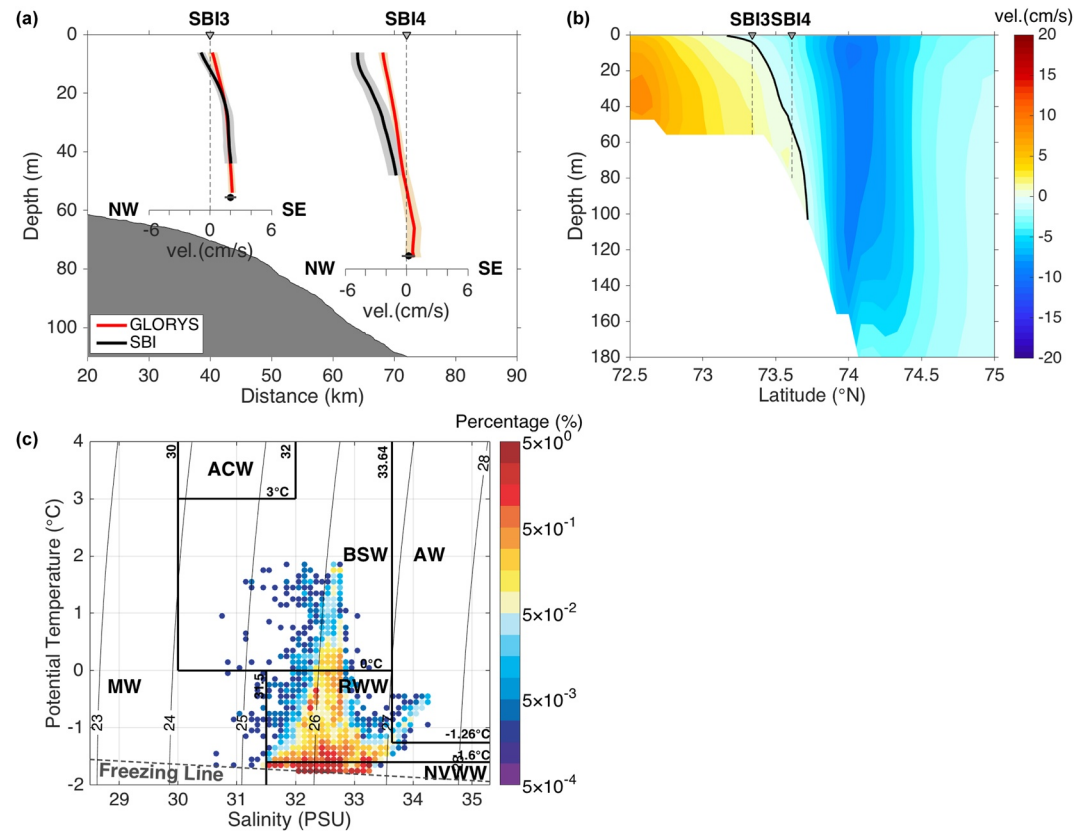
Figure 4. (a) Two-year mean alongstream velocity profiles (black curves for ADCP and black dots for RCM) with standard error (shading) at SBI3 and SBI4 from mooring observations (black) and the GLORYS reanalysis (red). (b) Two-year mean alongstream velocity section at 166°W from GLORYS. The black line is the zero contour. (c) Potential temperature-salinity diagram for all of the hydrographic data (three CTDs) on the two SBI moorings. The color denotes the percentage of the water within a 0.1°C by 0.1 salinity grid. The dashed line is the freezing line (reference pressure at sea surface). The boundaries of the water masses are indicated by black lines. MW = melt water and runoff and precipitation; ACW = Alaskan Coastal Water, BSW = Bering Summer Water; RWW = Remnant Winter Water; NVWW = Newly-Ventilated Winter Water; AW = Atlantic Water.

in Figure 4b. This reveals a southeastward-flowing bottom-intensified current in the vicinity of the shelfbreak and a northwestward-flowing surface-intensified flow offshore—that is, the Chukchi Shelfbreak Jet adjacent to the Chukchi Slope Current. This is similar to the composite vertical section of alongstream velocity constructed by Corlett and Pickart (2017) using shipboard ADCP data, as well as the 1-year mean velocity section from the Chukchi slope mooring array just west of Barrow Canyon presented in Li et al. (2019). The location of the SBI moorings is indicated on the mean velocity section from the GLORYS reanalysis (Figure 4b), showing that, in the mean, the SBI3 mooring was located at the offshore edge of the Chukchi Shelfbreak Jet, while the SBI4 mooring was located at the inshore edge of the Chukchi Slope Current. In sum, the mooring observations, supported by the GLORYS data, provide clear evidence that the Chukchi Slope Current persists to at least 166°W (~400 km west of Barrow Canyon).

The CTD on SBI3 (61 m) and two CTDs on SBI4 (56 and 96 m) are used to investigate the water properties present during the deployment period. Following Corlett and Pickart (2017) and Li et al. (2019), we consider six water masses (see Table 2 for the definitions): the warm Alaskan Coastal Water (ACW) and moderately warm Bering Summer Water (BSW), the cold Newly-Ventilated Winter Water (NVWW) and moderately cold Remnant Winter Water (RWW), the fresh Melt Water (MW) which includes runoff, precipitation, and river water, and the salty Atlantic Water (AW). The percent occurrence in potential temperature-salinity space for the 2-year period (Figure 4c) reveals that the dominant water masses were NVWW, RWW, and BSW, while MW and AW were relatively rare (0.1% and 0.5% respectively) and ACW was not present at all. This latter point is not a surprise since very little ACW was measured at the mooring array reported on by Li et al. (2019) located closer to Barrow Canyon (157°W), and the same was true for the collection of shipboard CTD sections occupied between Barrow Canyon and 168°W analyzed by Corlett and Pickart (2017).

Table 2
Definition of the Water Masses Considered in the Study

| Watermass type	Definition
Alaskan Coastal Water (ACW)	$T > 3°C$ and $30 < S < 32$
Bering Summer Water (BSW)	$0°C < T < 3°C$ and $30 < S < 32$
	$T > 0°C$ and $32 < S < 33.64$
Newly-Ventilated Winter Water (NVWW)	$T < −1.6°C$ and $S > 31.5$
Remnant Winter Water (RWW)	$−1.6°C < T < 0°C$ and $31.5 < S < 33.64$
	$−1.6°C < T < −1.26°C$ and $S > 33.64$
Melt Water and river runoff (MW)	$S < 30$; $T < 0°C$ and $30 < S < 31.5$
Atlantic Water (AW)	$T > −1.26°C$ and $S > 33.64$

Note. T and S denote the potential temperature and salinity, respectively.

3.3. Seasonality

The seasonal mean alongstream velocity over the 2 years at SBI3 and SBI4 showed relatively little variation (Figure 5), although there were some variations of note. The current at SBI3 was weak for each season of the 2 years except for the two autumns when the bottom-intensified flow of the Chukchi Shelfbreak Jet was enhanced (roughly twice as strong, increasing from 2 cm s^{-1} to 4 cm s^{-1}). The current at SBI4 was surface intensified to the northwest in each season. It is notable that the standard error was significantly larger during the fall (true for both
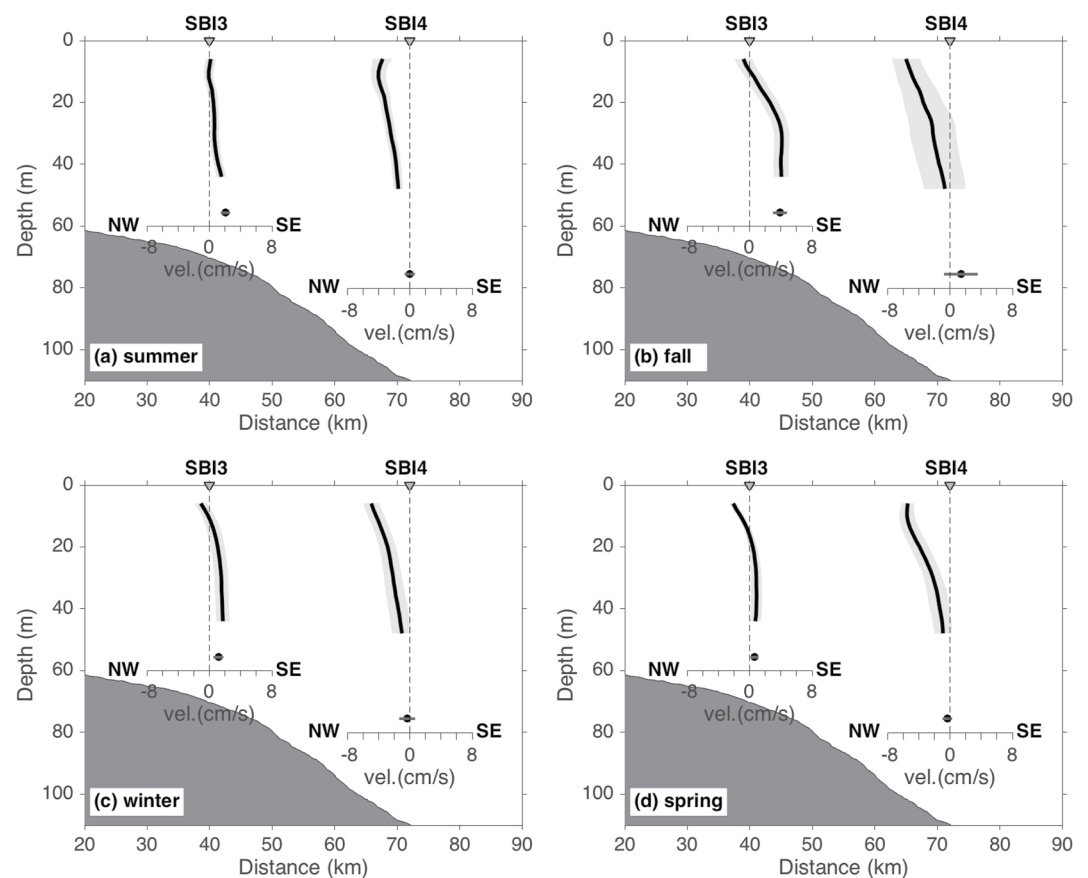
Figure 5. Seasonal mean velocity profiles at SBI3 and SBI4, with the standard error shaded (the presentation is the same as in Figure 4a). (a) Summer: June–July–August; (b) fall: September–October–November; (c) winter: December–January–February; (d) spring: March–April–May.
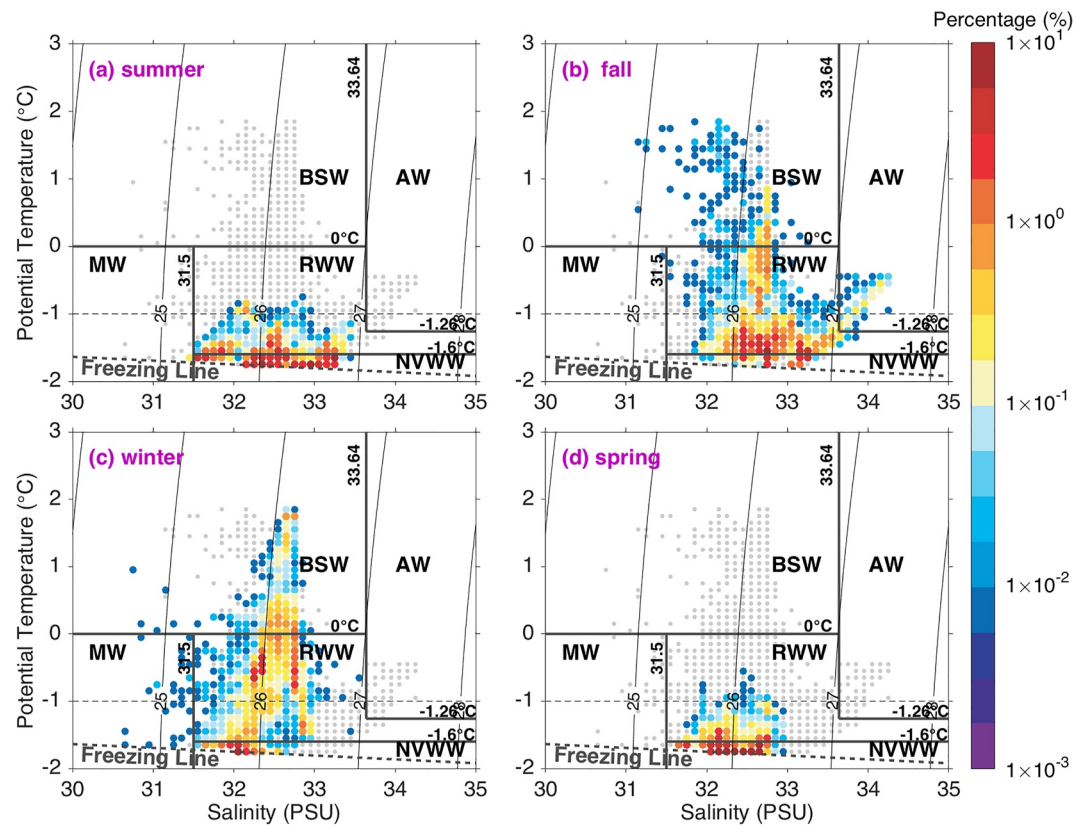
Figure 6. Same as Figure 4c, except for (a) summer: June–July–August, (b) fall: September–October–November, (c) winter: December–January–February, and (d) spring: March–April–May. The gray dots denote all data from the other seasons. The bold and light dashed lines denote the freezing line and −1°C, respectively.

years), with a maximum of 2.9 cm s^{-1} (Figure 5b). This may be related to the strong extreme states of the current (see Section 3.4 below). The lack of seasonality at SBI4 may seem surprising in light of the mooring results of Li et al. (2019) who showed that the Chukchi Slope Current varies in both strength and position over the course of the year. However, one should keep in mind that SBI4 was located at the inshore edge of the Chukchi Slope Current, and inspection of the equivalently placed mooring from the eastern array (see Li et al., 2019) showed a similarly steady flow structure. Therefore, it is probable that the weak seasonality at SBI4 was due to its location being shoreward of the core of the Chukchi Slope Current.

Figure 6 shows the seasonality of the water masses. BSW was only present in fall and winter, while the percentages of NVWW in fall and winter were less than those in spring and summer. Most of the RWW in spring (98.6%) and summer (94.8%) was cold and close to NVWW, while a notable portion of RWW in fall (19.2%) and winter (77%) was warmer than −1°C and close to BSW. The latter might in part be due to a mixture of BSW and the previous cold RWW. A small amount of AW (2.1%) appeared in the fall; this is likely water that was upwelled to the upper slope from the deep layer during the fall storm season (e.g., Woodgate, Aagaard, Swift, et al., 2005).

3.4. Dominant Modes of Velocity

The correlation coefficient between the depth-averaged alongstream ADCP velocities at SBI3 and SBI4 is 0.53 ($p < 0.05$), revealing a significant covariability between them. To investigate this, we carried out a coupled EOF analysis on the alongstream velocities at the two moorings. The first mode explained 69% of the variance (Figure 7). The spatial structure of EOF1 is similar at both mooring sites, with very little depth variation, suggesting the currents at the two moorings vary in phase (Figure 7a). The PC1 timeseries (Figure 7b) reveals variability on a wide range of time scales, including energetic synoptic variability.
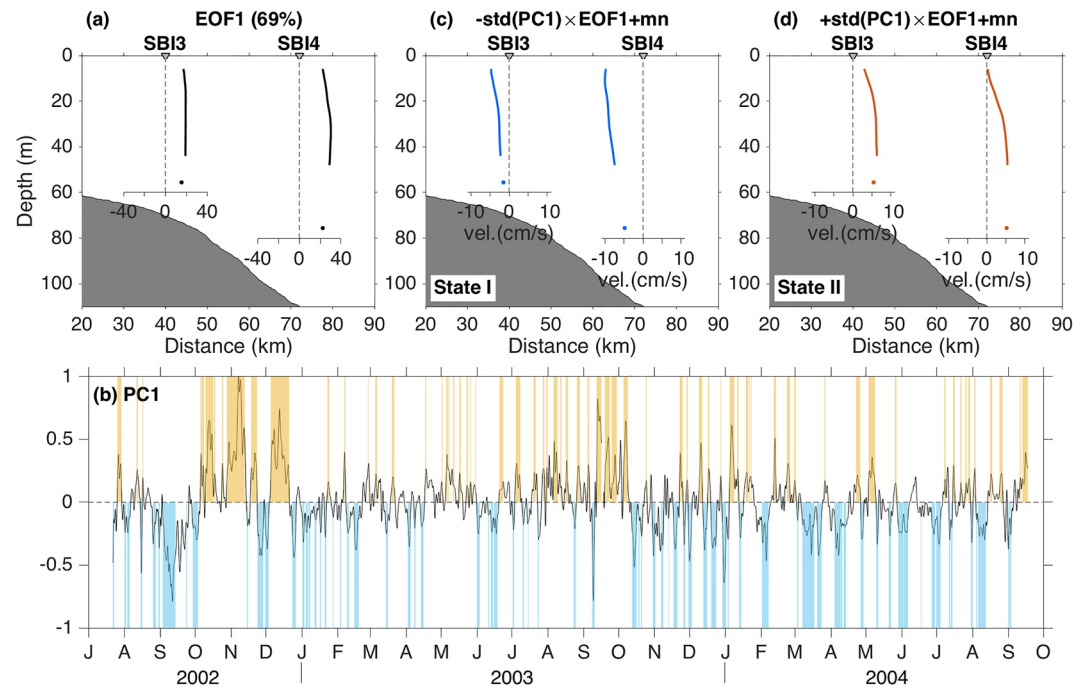
Figure 7. (a) Spatial structure of EOF mode 1 of alongstream velocity at the two SBI mooring sites. (b) The principal component timeseries PC1 for EOF mode 1. This has been normalized such that the value of the profiles in (a) represent the maximum dimensional values of the mode in cm s^{-1}. The yellow and blue shading in (b) indicate instances of the two flow extremes discussed in Section 3.4 (yellow: strong southeastward flow; blue: strong northwestward flow). (c) State I: EOF1 multiplied by negative one standard deviation of PC1, added to the 2-year mean profile; (d) State II: Same as (c) except for positive one standard deviation of PC1.

To more clearly depict the impact of the mode on the velocity, we multiplied the modal structure of EOF1 by positive/negative one standard deviation of PC1 and then added that to the 2-year mean profile, resulting in reconstructed velocity profiles at moorings SBI3 and SBI4 for the two states. These are referred to as state I and state II, which represent the two dominant configurations of the alongstream velocity field (Figures 7c and 7d). In state I, the currents at both sites are surface-intensified and flowing to the northwest (Figure 7c), while in state II they are directed southeastward with stronger flow at depth (Figure 7d).

These two configurations of mode 1 are reminiscent of the two extreme states identified by Li et al. (2019) using timeseries from the shelf-slope mooring array just west of Barrow Canyon. To determine whether a similar situation occurs at this longitude (300 km farther to the west), we applied an analogous method to that used by Li et al. (2019) to identify the two extreme states, except that alongstream velocity is used here instead of volume transport. The condition of strong northwestward flow (state I) is defined as times when the depth-mean alongstream velocity at SBI4 is less than the 2-year mean minus 0.3 × the standard deviation (i.e., strongly negative) and, at the same time, the alongstream velocity at SBI3 is smaller than its 2-year mean minus 0.3 × the standard deviation (i.e., weakly positive or reversed). We tried different values, and a value of 0.3 resulted in the most sensible results in terms of the duration of the extreme events. Conversely, the condition of strong southeastward flow (state II) is defined as when the alongstream velocity at SBI3 is larger than its 2-year mean plus 0.3 × the standard deviation (i.e., strongly positive) and the alongstream velocity at SBI4 is larger than its 2-year mean plus 0.3 × the standard deviation (i.e., weakly negative or reversed). Occurrences of the two flow states are marked using blue shading (state I) and yellow shading (state II) in Figure 7b. Note that the two states defined as such correspond well to negative and positive peaks of PC1.

A total of 73 events (37 in the first year and 36 in the second year) corresponding to state I were identified, occupying 21.6% of the full record. The composite average of the alongstream velocity for these 73 events (Figure 8a) shows surface-intensified northwestward flow at both mooring sites with a velocity maximum of 10 cm s^{-1} (6 cm s^{-1}) at the upper-slope (outer-shelf) site. This is similar to the reconstructed velocity profiles for the negative state of the EOF mode (compare Figures 8a and 7c). The velocity anomaly relative to the 2-year
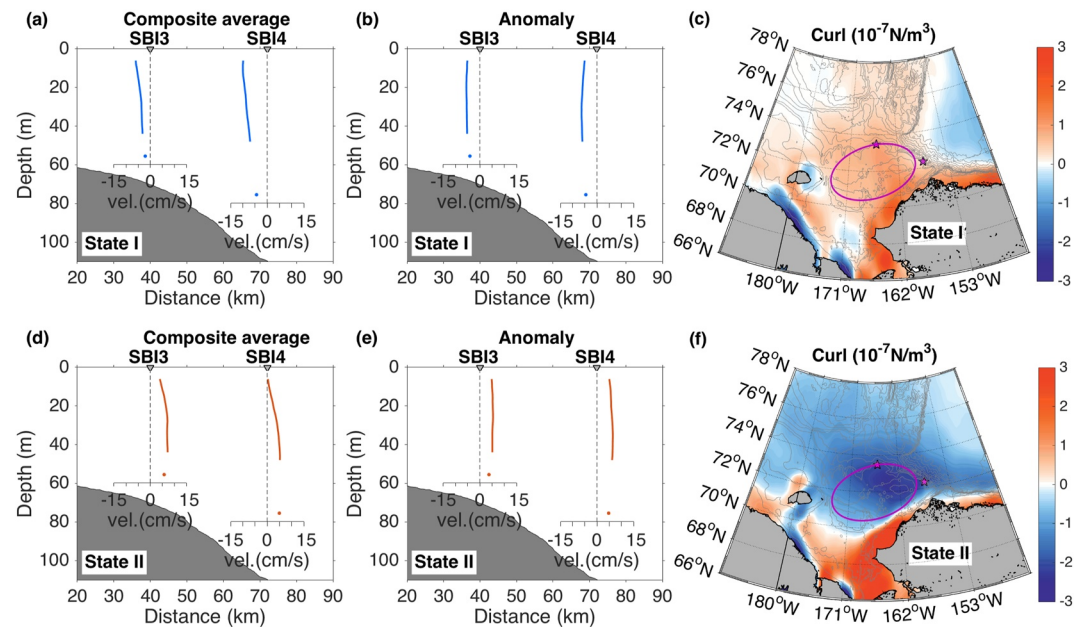
Figure 8. Composite average profiles of (a, d) alongstream velocity, and (b, e) alongstream velocity anomaly relative to the 2-year mean, for the two extreme states (see text for details). (c, f) Composite average fields of wind stress curl for the two states. In (c) and (f), the purple stars in the west and east denote the locations of the SBI mooring array analyzed here and the shelf/slope mooring array analyzed by Li et al. (2019), respectively. The purple ellipses denote the same shelf region considered by Li et al. (2019).

mean was similar for both sites (∼5 cm s⁻¹; Figure 8b). For state II, 67 events (36 for the first year and 31 for the second year) were identified, totaling 20.1% of the full record. The associated composite average reveals bottom-intensified southeastward flow and positive anomaly relative to the 2-year mean at each site (Figures 8d and 8e), similar to the reconstructed modal velocity structure in Figure 7d.

Li et al. (2019) demonstrated that the wind stress curl over the Chukchi shelf is the dominant driver of the synoptic variability of the Chukchi Shelfbreak Jet and Chukchi Slope Current just west of Barrow Canyon. Positive wind stress curl lowers the sea surface height (SSH) on the shelf through Ekman divergence, and the enhanced northward gradient in SSH across the slope results in anomalously stronger geostrophic flow to the northwest. By contrast, negative wind stress curl raises the SSH on the shelf through Ekman convergence, causing a reduced northward gradient across the slope and anomalously weaker geostrophic flow to the northwest. This motivated us to consider the wind stress curl field in order to see if similar dynamics were at work at this location. The composite averaged wind stress curl for the two extreme states are shown in Figures 8c and 8f. This demonstrates clearly that the wind stress curl on the shelf (within the region of the purple ellipse) was strongly positive for the enhanced northwestward flow state and was strongly negative for the opposite state, suggesting the same influence of the wind stress curl on the intensity of the two boundary currents as was found farther to the east by Li et al. (2019).

We note that the SBI mooring data alone are not sufficient to arrive at this conclusion. Because the two moorings are situated close to the dividing line between the Chukchi Shelfbreak Jet and Chukchi Slope Current (Figure 4b), one interpretation of the two states identified here could be that there was a lateral shift in the location of the two currents, with no change to their magnitude. Alternatively, there could have been a strengthening/widening of the Chukchi Shelfbreak Jet with no change in the core speed of the Chukchi Slope Current, or vice versa. However, the EOF and extreme state results presented here, in tandem with the wind stress curl composites, strongly suggest that this is the same mode of variability identified by Li et al. (2019) farther to the east. To shed light on this, we performed an analogous EOF calculation using the two equivalent moorings from the eastern array: the mooring just inshore of the shelfbreak and the mooring on the upper slope (moorings CS2 and CS3 in Li et al., 2019). EOF mode 1 using only these two moorings was similar in both structure and variance explained to EOF mode 1 presented here.

The second EOF mode explained 20% of the variance (far less than the 69% explained by mode 1), with an out-of-phase spatial structure between SBI3 and SBI4 (not shown). Interestingly, the corresponding PC2 did not display any seasonal variation, unlike the clear seasonality of PC2 from the EOF analysis of Li et al. (2019) using the five-mooring array farther to the east. However, EOF 2 using two equivalent moorings from the eastern array does give a similar result of no clear seasonality. This indicates that, while two moorings placed as such are sufficient to capture the two extreme states of the Chukchi Shelfbreak Jet and Chukchi Slope Current driven by the wind stress curl, they are unable to capture the seasonal variability. This is likely because two moorings thusly situated are too far away from the cores of the two currents, consistent with the results presented above in Section 3.3.

4. Hydrographic Implications

We now investigate the relationship between the hydrographic signals at the two moorings and the circulation, including the origin of the water present in the Chukchi Shelfbreak Jet and Chukchi Slope Current. For the latter we use mooring data from Herald Canyon (MF2) and Barrow Canyon (BC1).

4.1. Local Water Masses and Currents

Timeseries of potential temperature at the different depth levels at the two SBI mooring sites are presented in Figures 9a and 9c, where data from the thermistors on the RCMs and ADCPs are included. Recall that the water depths at SBI3 and SBI4 are ~71 and ~108 m, respectively (Table 1). Based on the water mass definitions presented in Figure 4c and Table 2, we have also constructed a water mass record at each of the CTD locations (Figures 9b, 9d, and 9e). Relatively warm water $>-1°C$ (occasionally exceeding 1°C) appeared at SBI3 and SBI4 from late-fall to winter, revealing an annual variability at both sites during the 2 years (see also Figure 6). To investigate the relationship between this warm water and the currents, the alongstream velocities obtained from the RCM or the depth bin of the ADCP closest to the temperature sensor from October to February are presented in Figure 10.

At SBI3, the water mass timeseries shows that the relatively warm water with temperature $>-1°C$ was mainly RWW and BSW (Figure 9b; the grayish blue and green bands, respectively). In the first year (2002), the temperature increased synchronously at all three depth levels in early November. The velocity vectors at 44 and 56 m (Figures 10a and 10b) both revealed frequent and strong eastward/southeastward flow from October to November 2002, suggesting that the warm water in November was associated with this enhanced flow. A similar pattern of warm water arrival and enhanced eastward flow in fall occurred in the second year as well (Figures 10e and 10f).

At SBI4, the temperature at 52 and 56 m showed a nearly simultaneous warming with SBI3 in November 2002 (Figure 9c), suggesting that this site was initially influenced by the same eastward flow as that occurring at SBI3. This is corroborated by similarly strong eastward velocity vectors at SBI4 during this time (Figures 10c and 10d). However, the current at SBI4 veered to the northwest in mid-December 2002 (Figures 10c and 10d), distinct from the flow at SBI3. Moreover, in the second winter the water at SBI4 mainly flowed northwestward when the temperature increased in November and December 2003 (Figures 10g and 10h). At the deepest layer (96m), a pronounced period of warm BSW lasted from late January to early February 2004 (Figure 9e; the green bands) during which time the alongstream velocity was predominantly northwestward (Figure 10h). Hence, this implies that, aside from the brief period in November 2002 when the warm water at SBI3 and SBI4 flowed simultaneously to the southeast, the nature and origin of the warming at the two mooring sites were different.

### 4.2. Remote Water Mass Connections

It is of interest to consider the origins of the warm water measured at the SBI moorings. To address this, we focus on the BSW and use data from the moorings in Herald Canyon (MF2), Barrow Canyon (BC1), and on the northeastern slope (CS4, within the Chukchi Slope Current). The locations of these moorings are indicated in Figure 1. We note that not all of the timeseries are contemporaneous with the SBI mooring data, but we assume that the seasonal timing of the warm water is generally similar each year, which is the case for Barrow Canyon where there are long-term observations (Weingartner et al., 2017).
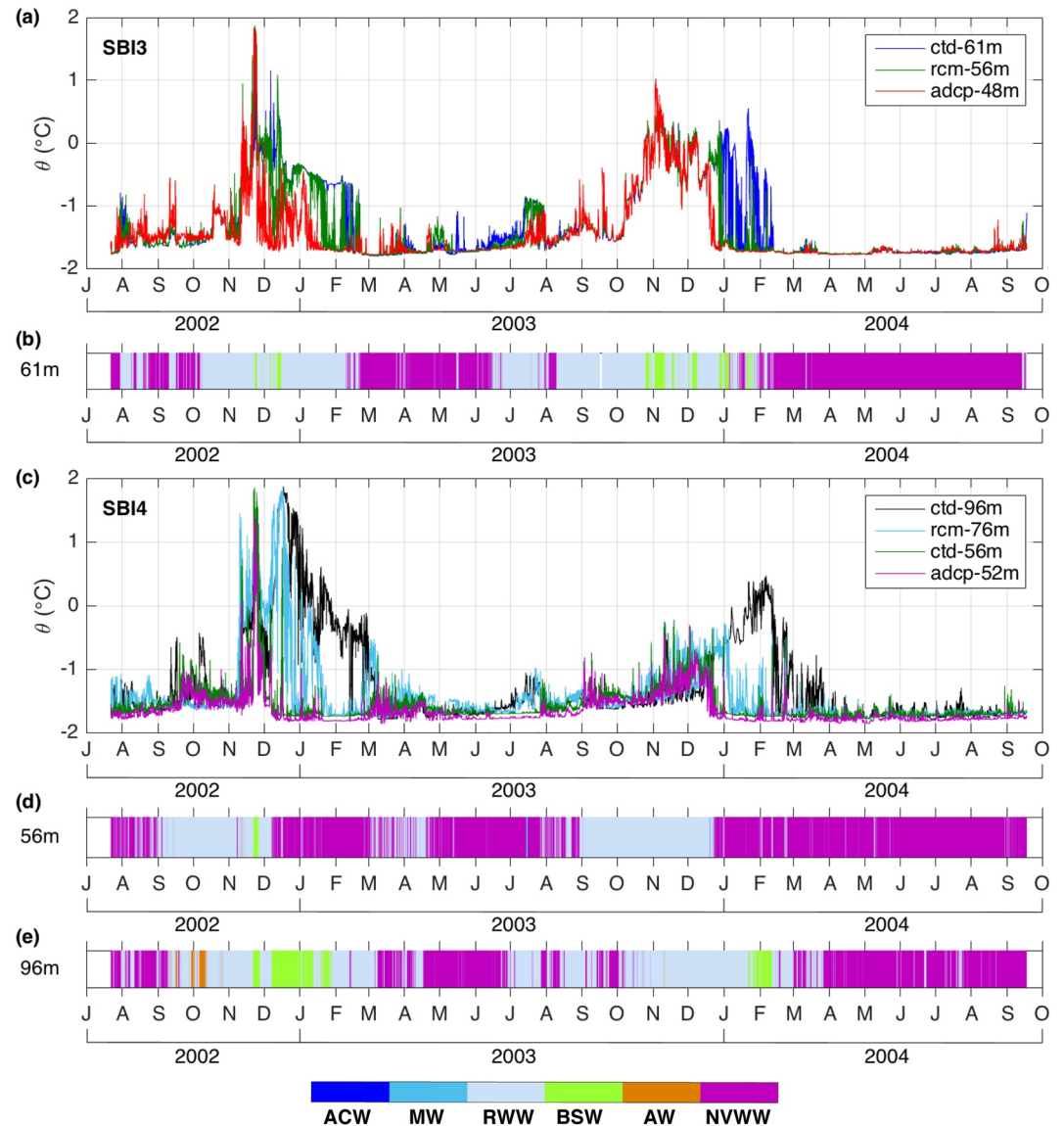
Figure 9. (a, c) Potential temperature timeseries at SBI3 and SBI4 measured by the thermistors on the CTDs, RCMs, and ADCPs with legends indicating instruments and depths on the right. (b) Water mass timeseries at 61 m at SBI3. (d, e) Same as (b) except for 56 and 96 m, respectively, at SBI4. The ACW, MW, RWW, BSW, AW, NVWW denote Alaskan Coastal Water, Melt Water, Remnant Winter Water, Bering Summer Water, Atlantic Water, and Newly-Ventilated Winter Water, respectively, which are defined in Figure 4c and Table 2.

4.2.1. Water From the West

Previous shipboard observations have revealed that warm Pacific-origin water on the eastern flank of Herald Canyon in summer and fall flows poleward, then turns to the east after exiting the canyon and forms the Chukchi Shelfbreak Jet along the northern edge of the Chukchi shelf (Linders et al., 2017; Pickart et al., 2010). The hydrographic and current meter data from mooring MF2 on the canyon's eastern flank during 1990–1991 indicate that the current was indeed directed northward during most of the BSW period (Figure 11c). From the water mass timeseries of Figure 11b, the BSW arrived in Herald Canyon near the beginning of September in 1991 (it was already there when the mooring was deployed in September 1990). From the water mass timeseries of Figure 9b, the BSW arrived at mooring SBI3 in the Chukchi Shelfbreak Jet near the beginning of December in 2002 and near the beginning of November in 2003 (indicated by the green bands). This implies a lag of between 55 and 80 days. The mean velocity at 56 m during the BSW period of mooring SBI3 for both years was 3.8 cm s^{-1}, while
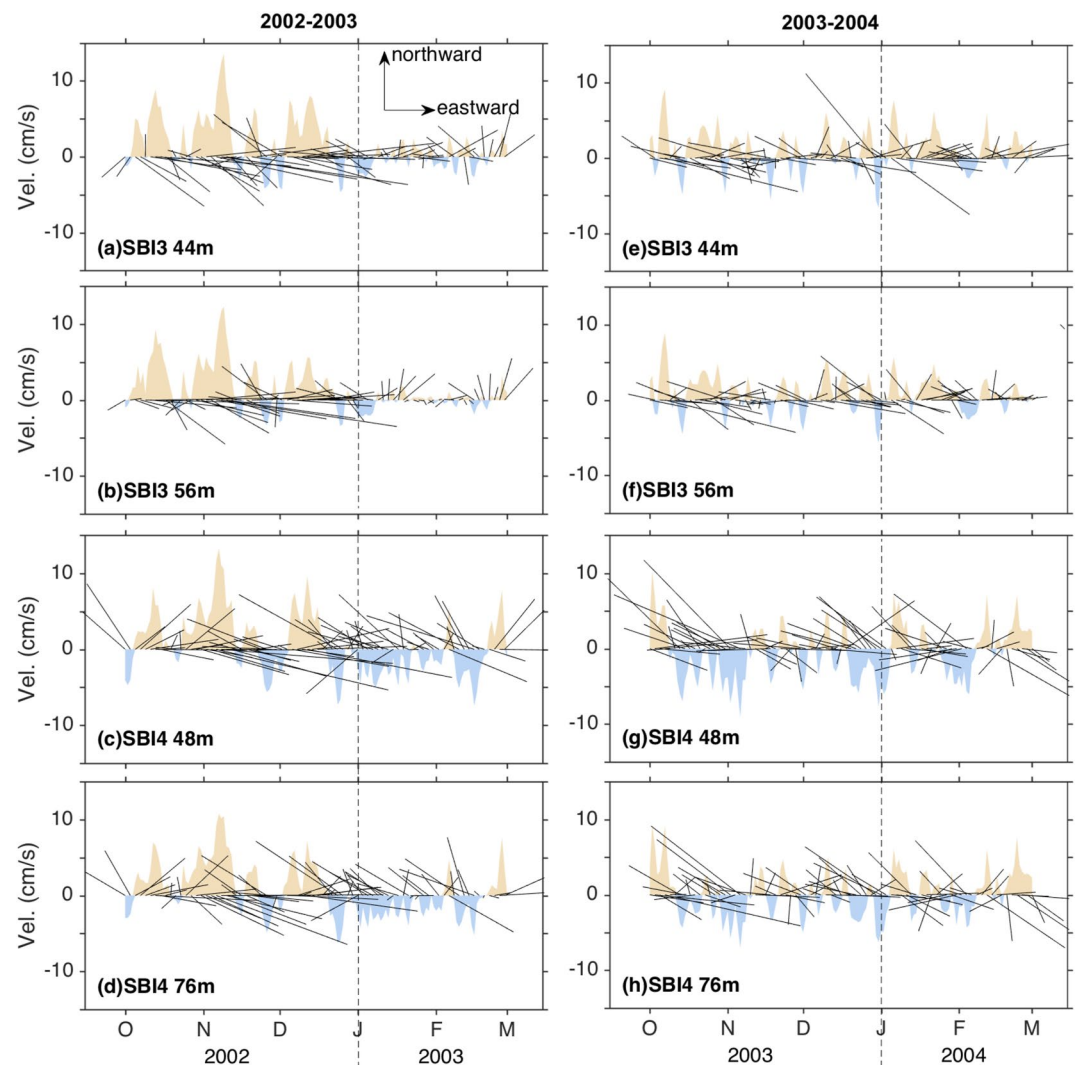
Figure 10. Timeseries of daily-averaged velocity vectors (black sticks; only every other vector is plotted) and alongstream velocity multiplied by 0.5 (shading; yellow: positive, blue: negative) at 44 m (a, e) and 56 m (b, f) of SBI3, and 48 m (c, g) and 76 m (d, h) of SBI4 from October 2002 to February 2003 (left panels) and SBI4 from October 2003 to February 2004 (right panels). The black dashed line denotes January 1st.

the mean velocity during the BSW period at MF2 was 18 cm s^{-1}. We assume that the latter value is representative of the full length of the canyon, while the former value applies to the Chukchi Shelfbreak Jet to the east of the canyon. The distance between MF2 and the mouth of Herald Canyon is ∼200 km, and the distance between the mouth of Herald Canyon and SBI3 is ∼300 km. Taking the distance-weighted velocity, 9.5 cm s^{-1}, as a rough estimate of the advective speed between MF2 and SBI3, together with the distance between the two locations (∼500 km), gives a transit time of approximately 60 days for the BSW to reach SBI3, which falls in the middle of the time lag range estimated from the water mass timeseries. Admittedly there are significant assumptions in this calculation, but the result suggests that this route is the likely pathway for the warm water.

4.2.2. Water From the East

The westward-flowing BSW at SBI4 is presumably warm Pacific-origin water that originated from Barrow Canyon and was carried by the Chukchi Slope Current to the mooring site. To investigate this, we examined the relationship between the temperature at 67 m at the head of Barrow Canyon, where mooring BC1 was deployed from August 2002 to September 2004 (as part of the SBI program), and the temperature at 96 m at SBI4.
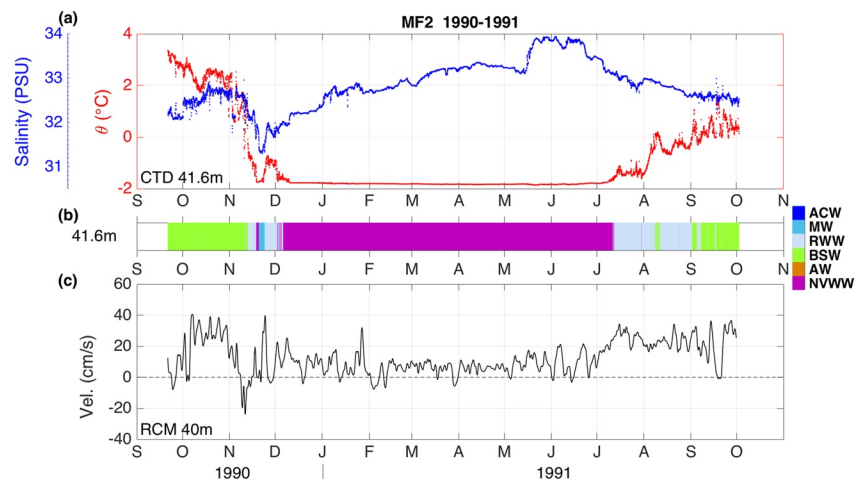
Figure 11. (a) Potential temperature (red dots), salinity (blue dots), (b) water mass, and (c) alongstream velocity timeseries from the mooring in Herald Canyon during 1990–1991. The watermass colorbar in panel (b) is the same as that in Figure 9. The alongstream direction is defined as 357°T based on the year-long mean vector.

In the fall of 2002 there was a similar amount of ACW (blue bands) as that of the BSW (green bands) measured at the head of Barrow Canyon (Figure 12b). Using shipboard data, Pickart et al. (2019) demonstrated that ACW is readily cooled and converted to BSW on the northeast Chukchi shelf in the month of October when the air temperature cools and winds are enhanced. Hence it is not unreasonable to assume that the later arriving ACW in October measured by mooring BC1 was similarly converted to BSW as it transited from the area. During the second year, BSW appeared at the head of the canyon in early October. At SBI4 at 96 m, BSW appeared in early December in the first year and in late-January the second year (Figure 9e; green bands). This implies a lag of between 60 and 115 days between the two locations, since the BSW (including that converted from ACW) was present in the canyon in early October and appeared at SBI4 in early-December/late-January. To estimate the advective time of the BSW we use the velocity records representative for this water mass transiting from BC1 to CS4 (mean of 10.7 cm s^{-1} for the single year that the mooring was deployed), and use velocity records at SBI4 for BSW transiting from CS4 to SBI4 (mean of 1.3 cm s^{-1} for the 2 years). Based on the distance between the sites (~300 km between BC1 and CS4, and ~300 km between CS4 and SBI4), this gives a transit time of approximately 90 days. This is again within the time lag range estimated from the water mass timeseries.
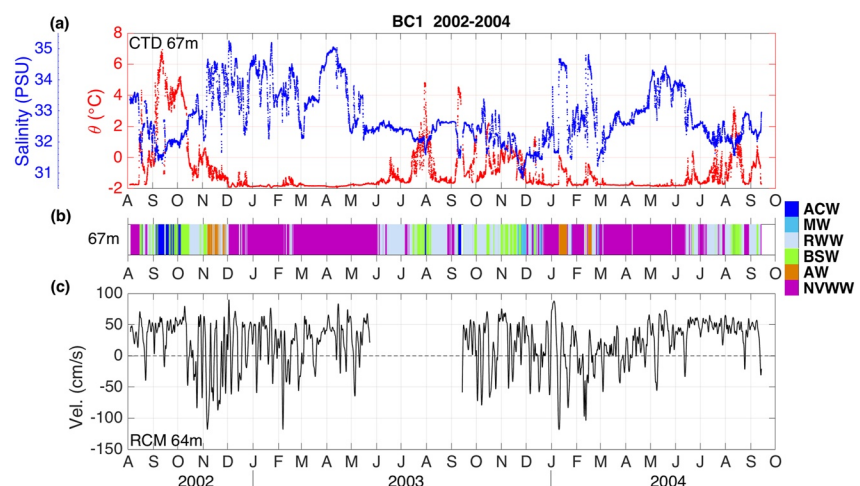
Figure 12. Same as Figure 11 except for the mooring in Barrow Canyon during 2002–2004. The alongstream direction is defined as 59.6°T based on the two year mean vector. The watermass colorbar in panel (b) is the same as that in Figure 9. (There are no velocity data from 24 May to 14 September 2003, see Table 1.)

Previous studies have investigated the transport of BSW by the Chukchi Slope Current in winter. The temperature record from a mooring on the Chukchi continental slope revealed the passage of warm BSW during winter 2016, which was linked to the Barrow Canyon outflow (Kimura et al., 2019). The water mass took 10–20 days to travel the 70 km distance from the Barrow Canyon site to the mooring on the slope. Extrapolating this result to the location of SB4 gives a qualitatively similar transmit time as that estimated here. We note that such an advective time is longer than that deduced from the surface drifter results of Stabeno and McCabe (2020). This difference could be explained by seasonality since the drifters were operational in summer and early fall (Stabeno et al., 2018) when the currents are stronger both in Barrow Canyon and along the Chukchi slope (Itoh et al., 2013; Li et al., 2019; Stabeno & McCabe, 2020).

5. Summary

Data from two moorings deployed from 2002 to 2004 as part of the SBI program at 166°W were analyzed to investigate the boundary currents and water masses along the northern Chukchi Shelfbreak and slope. The 2-year mean velocity vectors and alongstream velocity profiles showed that the mean current was northeastward at the outer-shelf mooring (SBI3) and northwestward at the upper-slope mooring (SBI4). This, together with the corresponding mean velocity section constructed using the GLORYS12V1 data-assimilating ice-ocean reanalysis data, suggests that SBI3 was located at the seaward edge of the Chukchi Shelfbreak Jet while SBI4 was located at the shoreward edge of the Chukchi Slope Current.

The dominant alongstream velocity variability at the two moorings was analyzed using an EOF analysis. The first mode, which explains 69% of the variance, revealed two types of extreme events: (a) the Chukchi Slope Current is strongly northwestward at SBI4 while the Chukchi Shelfbreak Jet current is weakly southeastward or reversed to the northwest at SBI3; and (b) the Chukchi Shelfbreak Jet is strongly southeastward at SBI3 while the Chukchi Slope Current is weakly northwestward or reversed to the southeast at SBI4. These states occupied 21.6% and 20.1% of the full 2-year timeseries, respectively. The analysis of the ERA5 atmospheric reanalysis data revealed that this synoptic variability is due to the influence of the wind stress curl on the Chukchi shelf via Ekman dynamics and geostrophic set up, analogous to the dynamics of both currents closer to Barrow Canyon near 157°W (Li et al., 2019).

The mooring data show that NVWW, RWW, and BSW were three main water masses present at the mooring site, with only a small fraction of AW and MW. It is important to keep in mind, however, that there were no temperature/salinity sensors shallower than 48 m and thus lighter water masses may have been missed by the moorings. The hydrographic data revealed annual warm water signals at both moorings in late fall and winter, during which BSW with temperature >0°C was present. Using ancillary mooring data from Herald Canyon (a decade earlier), Barrow Canyon (in the same years), and farther east on the Chukchi continental slope (a decade later), we argue that the eastward-flowing BSW at SBI3 likely stemmed from the outflow of Herald Canyon, while the westward-flowing BSW at SBI4 likely originated from the outflow of Barrow Canyon.

Our results provide the first robust evidence that the Chukchi Slope Current is a persistent feature this far west of Barrow Canyon. Together with findings from previous studies (e.g., Boury et al., 2020; Leng et al., 2021; Lin et al., 2021), this supports the notion that the current bifurcates downstream of Barrow Canyon, with some of the flow heading northward around the edge of the Beaufort Gyre and some of it heading westward along the continental slope toward the East Siberian Sea. Unfortunately, the SBI mooring data had insufficient spatial coverage for computing alongstream volume transports, so the degree to which the Chukchi Slope Current splits upstream still needs to be determined. In hindsight, the placement of the two SBI moorings was unfortunate in that they were located near the edges of the two currents (to be fair, the existence of the Chukchi Slope Current was unknown at that point). Going forward, a mooring array that samples the full extent of the Chukchi Slope Current is required to shed more light on the fate of the Pacific-origin water in the Arctic Ocean.

Data Availability Statement

The mooring data can be found at the following sites: SBI3-4 moorings: https://doi.org/10.5065/D64747X3; CS4 mooring: https://www.boem.gov; MF2 mooring: http://psc.apl.washington.edu/Chukchi.html; BC1 mooring: https://doi.org/10.5065/D62805QS.

References

Boury, S., Pickart, R. S., Odier, P., Lin, P., Li, M., Fine, E. C., et al. (2020). Whither the Chukchi slope current? *Journal of Physical Oceanography*, *50*(6), 1717–1732. https://doi.org/10.1175/jpo-d-19-0273.1

Brugler, E. T., Pickart, R. S., Moore, G. W. K., Roberts, S., Weingartner, T. J., & Statscewich, H. (2014). Seasonal to interannual variability of the Pacific water boundary current in the Beaufort Sea. *Progress in Oceanography*, *127*, 1–20. https://doi.org/10.1016/j.pocean.2014.05.002

Corlett, W. B., & Pickart, R. S. (2017). The Chukchi slope current. *Progress in Oceanography*, *153*, 50–65. https://doi.org/10.1016/j.pocean.2017.04.005

Emery, W. J., & Thomson, R. E. (2001). *Data analysis methods in physical oceanography* (second and revised edition, p. 638). Elsevier.

Foukal, N. P., Pickart, R. S., Moore, G. W. K., & Lin, P. G. (2019). Shelfbreak downwelling in the Alaskan Beaufort sea. *Journal of Geophysical Research-Oceans*, *124*(10), 7201–7225. https://doi.org/10.1029/2019jc015520

Gong, D., & Pickart, R. S. (2015). Summertime circulation in the eastern Chukchi Sea. *Deep-Sea Research II*, *118*, 18–31. https://doi.org/10.1016/j.dsr2.2015.02.006

Håvik, L., Våge, K., Pickart, R. S., Harden, B., Appen, W. J. V., Jónsson, S., & Østerhus, S. (2017). Structure and variability of the shelfbreak east Greenland current north of Denmark strait. *Journal of Physical Oceanography*, *47*(10), 2631–2646. https://doi.org/10.1175/jpo-d-17-0062.1

Hill, V. J., & Cota, G. F. (2005). Spatial patterns of primary production on the shelf, slope and basin of the Western Arctic in 2002. *Deep-Sea Research II*, *52*(24–26), 3344–3354. https://doi.org/10.1016/j.dsr2.2005.10.001

IPCC Special Report on Ocean and Cryosphere. (2019). Retrieved from http://www.ipcc.ch/srocc/

Itoh, M., Nishino, S., Kawaguchi, Y., & Kikuchi, T. (2013). Barrow Canyon volume, heat, and freshwater fluxes revealed by long-term mooring observations between 2000 and 2008. *Journal of Geophysical Research: Oceans*, *118*(9), 4363–4379. https://doi.org/10.1002/jgrc.20290

Jean-Michel, L., Greiner, E., Bourdallé-Badie, R., Gilles, G., Angelique, M., Marie, D., et al. (2021). The Copernicus global 1/12° oceanic and sea ice GLORYS12 reanalysis. *Frontiers in Earth Science*, *9*. https://doi.org/10.3389/feart.2021.698876

Jones, E. P., & Anderson, L. G. (1986). On the origin of the chemical properties of the Arctic Ocean halocline. *Journal of Geophysical Research*, *91*(C9), 10759–10767. https://doi.org/10.1029/JC091iC09p10759

Kimura, S., Onodera, J., Itoh, M., Kikuchi, T., Nishino, S., Kawaguchi, Y., et al. (2019). The warming of the Chukchi slope through the Barrow canyon outflow in the 2016–2017 winter. *Journal of Geophysical Research: Oceans*, *124*(11), 7437–7456. https://doi.org/10.1029/2019jc015093

Leng, H., Spall, M. A., & Bai, X. (2022). Temporal evolution of a geostrophic current under sea ice: Analytical and numerical solutions. *Journal of Physical Oceanography*, *52*(6), 1191–1204. https://doi.org/10.1175/JPO-D-21-0242.1

Leng, H., Spall, M. A., Pickart, R. S., Lin, P., & Bai, X. (2021). Origin and fate of the Chukchi slope current using a numerical model and in-situ data. *Journal of Geophysical Research: Oceans*, *126*(5). https://doi.org/10.1029/2021jc017291

Li, M., Pickart, R. S., Spall, M. A., Weingartner, T. J., Lin, P., Moore, G. W. K., & Qi, Y. (2019). Circulation of the Chukchi Sea shelfbreak and slope from moored timeseries. *Progress in Oceanography*, *172*, 14–33. https://doi.org/10.1016/j.pocean.2019.01.002

Lin, P., Pickart, R. S., Moore, G. W. K., Spall, M. A., & Hu, J. (2019). Characteristics and dynamics of wind-driven upwelling in the Alaskan Beaufort Sea based on six years of mooring data. *Deep-Sea Research II*, *162*, 79–92. https://doi.org/10.1016/j.dsr2.2018.01.002

Lin, P., Pickart, R. S., Våge, K., & Li, J. (2021). Fate of warm Pacific water in the Arctic Basin. *Geophysical Research Letters*, *48*(20). https://doi.org/10.1029/2021gl094693

Linders, J., Pickart, R. S., Björka, G., & Moore, G. W. K. (2017). On the nature and origin of water masses in Herald canyon, Chukchi Sea: Synoptic surveys in summer 2004, 2008, and 2009. *Progress in Oceanography*, *159*, 99–114. https://doi.org/10.1016/j.pocean.2017.09.005

Llinás, L., Pickart, R. S., Mathis, J. T., & Smith, S. L. (2009). Zooplankton inside an Arctic Ocean cold-core eddy: Probable origin and fate. *Deep Sea Research Part II: Topical Studies in Oceanography*, *56*(17), 1290–1304. https://doi.org/10.1016/j.dsr2.2008.10.020

Mathis, J. T., Pickart, R. S., Hansell, D. A., Kadko, D., & Bates, N. R. (2007). Eddy transport of organic carbon and nutrients from the Chukchi Shelf: Impact on the upper halocline of the Western Arctic Ocean. *Journal of Geophysical Research*, *112*(C5), C05011. https://doi.org/10.1029/2006jc003899

Nikolopoulos, A., Pickart, R. S., Fratantoni, P. S., Shimada, K., Torres, D. J., & Jones, E. P. (2009). The Western arctic boundary current at 152°W: Structure, variability, and transport. *Deep-Sea Research II*, *56*(17), 1164–1181. https://doi.org/10.1016/j.dsr2.2008.10.014

Onarheim, I. H., Eldevik, T., Smedsrud, L. H., & Stroeve, J. C. (2018). Seasonal and regional manifestation of Arctic sea ice loss. *Journal of Climate*, *31*(12), 4917–4932. https://doi.org/10.1175/jcli-d-17-0427.1

Paquette, R. G., & Bourke, R. H. (1974). Observations on the coastal current of Arctic Alaska. *Journal of Marine Research*, *32*, 195–207.

Pickart, R. S. (2004). Shelfbreak circulation in the Alaskan Beaufort sea: Mean structure and variability. *Journal of Geophysical Research*, *109*(C4), C04024. https://doi.org/10.1029/2003JC001912

Pickart, R. S., Nobre, C., Lin, P., Arrigo, K. R., Ashjian, C. J., Berchok, C., et al. (2019). Seasonal to mesoscale variability of water masses and atmospheric conditions in Barrow Canyon, Chukchi Sea. *Deep-Sea Research II*, *162*, 32–49. https://doi.org/10.1016/j.dsr2.2019.02.003

Pickart, R. S., Pratt, L. J., Torres, D. J., Whitledge, T. E., Proshutinsky, A. Y., Aagaard, K., et al. (2010). Evolution and dynamics of the flow through Herald canyon in the Western Chukchi Sea. *Deep-Sea Research II*, *57*(1–2), 5–26. https://doi.org/10.1016/j.dsr2.2009.08.002

Pickart, R. S., Spall, M. A., & Mathis, J. T. (2013). Dynamics of upwelling in the Alaskan Beaufort Sea and associated shelf-basin fluxes. *Deep-Sea Research I*, *76*, 35–51. https://doi.org/10.1016/j.dsr.2013.01.007

Pickart, R. S., Weingartner, T. J., Pratt, L. J., Zimmermann, S., & Torres, D. J. (2005). Flow of winter-transformed Pacific water into the Western Arctic. *Deep-Sea Research II*, *52*(24–26), 3175–3198. https://doi.org/10.1016/j.dsr2.2005.10.009

Pisareva, M. N., Pickart, R. S., Lin, P. G., Fratantoni, P. S., & Weingartner, T. J. (2019). On the nature of wind-forced upwelling in Barrow Canyon. *Deep-Sea Research I*, *162*, 63–78. https://doi.org/10.1016/j.dsr2.2019.02.002

Schulze, L. M., & Pickart, R. S. (2012). Seasonal variation of upwelling in the Alaskan Beaufort Sea: Impact of sea ice cover. *Journal of Geophysical Research*, *117*(C6), C06022. https://doi.org/10.1029/2012jc007985

Shimada, K., Kamoshida, T., Itoh, M., Nishino, S., Carmack, E., McLaughlin, F., et al. (2006). Pacific Ocean inflow: Influence on catastrophic reduction of sea ice cover in the Arctic Ocean. *Geophysical Research Letters*, *33*(8), L08605. https://doi.org/10.1029/2005GL025624

Spall, M. A., Pickart, R. S., Brugler, E. T., Moore, G. W. K., Thomas, L., & Arrigo, K. R. (2014). Role of shelfbreak upwelling in the formation of a massive under-ice bloom in the Chukchi Sea. *Deep-Sea Research II*, *105*, 17–29. https://doi.org/10.1016/j.dsr2.2014.03.017

Spall, M. A., Pickart, R. S., Fratantoni, P. S., & Plueddemann, A. J. (2008). Western Arctic shelfbreak eddies: Formation and transport. *Journal of Physical Oceanography*, *38*(8), 1644–1668. https://doi.org/10.1175/2007jpo3829.1

Spall, M. A., Pickart, R. S., Li, M., Itoh, M., Lin, P., Kikuchi, T., & Qi, Y. (2018). Transport of Pacific water into the Canada Basin. *Journal of Geophysical Research: Oceans*, *123*(10), 7453–7471. https://doi.org/10.1029/2018JC013825

Stabeno, P., Kachel, N., Ladd, C., & Woodgate, R. (2018). Flow patterns in the eastern Chukchi Sea: 2010-2015. *Journal of Geophysical Research: Oceans*, *123*(2), 1177–1195. https://doi.org/10.1002/2017jc013135

Stabeno, P. J., & McCabe, R. M. (2020). Vertical structure and temporal variability of currents over the Chukchi Sea continental slope. *Deep-Sea Research II*, *177*, 104805. https://doi.org/10.1016/j.dsr2.2020.104805

Steele, M., Morison, J., Ermold, W., Rigor, I., Ortmeyer, M., & Shimada, K. (2004). Circulation of summer Pacific halocline water in the Arctic Ocean. *Journal of Geophysical Research*, *109*(C2), C02027. https://doi.org/10.1029/2003jc002009

Teledyne RD Instruments. (2011). Acoustic Doppler current profiler principles of operation: A practical primer (p. 56). P/N 951-6069-00.

Weingartner, T., Aagaard, K., Woodgate, R., Danielson, S., Sasaki, Y., & Cavalieri, D. (2005). Circulation on the north central Chukchi Sea shelf. *Deep-Sea Research Part II*, *52*(24–26), 3150–3174. https://doi.org/10.1016/j.dsr2.2005.10.015

Weingartner, T. J., Potter, R. A., Stoudt, C. A., Dobbins, E. L., Statscewich, H., Winsor, P. R., et al. (2017). Transport and thermohaline variability in Barrow canyon on the northeastern Chukchi Sea shelf. *Journal of Geophysical Research: Oceans*, *122*(5), 3565–3585. https://doi.org/10.1002/2016jc012636

Woodgate, R. A., Aagaard, K., & Weingartner, T. J. (2005). A year in the physical oceanography of the Chukchi Sea: Moored measurements from autumn 1990–1991. *Deep-Sea Research II*, *52*(24–26), 3116–3149. https://doi.org/10.1016/j.dsr2.2005.10.016

Woodgate, R. A., Weingartner, T., & Lindsay, R. (2010). The 2007 Bering Strait oceanic heat flux and anomalous Arctic sea-ice retreat. *Geophysical Research Letters*, *37*(1), L01602. https://doi.org/10.1029/2009GL041621

Woodgate, R. A. K., Aagaard, J. H., Swift, K. K., Falkner, K. K., & Smethie, W. M. (2005). Pacific ventilation of the Arctic Ocean's lower halocline by upwelling and diapycnal mixing over the continental margin. *Geophysical Research Letters*, *32*(18), L18609. https://doi.org/10.1029/2005GL023999

Erratum

In the originally published version of this article, panels a and b in Figure 3 were incorrect because the wind rose in the opposite direction. In the corrected version of the figure, the wind rose in the direction where the wind blows from (which is consistent with the caption). The error has been corrected, and this may be considered the authoritative version of record.